

Drag Reduction in Turbulent Flows by Polymer and Fiber Additives[†]

Cristian Marchioli^{1,2*} and Marina Campolo¹

¹ Department of Engineering and Architecture, University of Udine, Italy

² International Center of Mechanical Sciences, Italy

Abstract

This article provides a review of the recent progress in understanding and predicting additives-induced drag reduction (DR) in turbulent wall-bounded shear flows. We focus on the reduction in friction losses by the dilute addition of high-molecular weight polymers and/or fibers to flowing liquids. Although it has long been reasoned that the dynamical interactions between polymers/fibers and turbulence are responsible for DR, it was not until recently that progress was made in elucidating these interactions in detail. Advancements come largely from numerical simulations of viscoelastic turbulence and detailed measurements in turbulent flows of polymer/fiber solutions. Their impact on current understanding of the mechanics and prediction of DR is discussed, and perspectives for further advancement of knowledge are provided.

Keywords: turbulence, drag reduction, polymers, fibers

1. Introduction

Over the last decades, there has been a steady increase in the number of scientific events and publications dedicated to the phenomenon of Drag Reduction (DR) in turbulent wall-bounded flows. The reduction in turbulent friction losses by the dilute addition of high-molecular weight polymers, fibers or other types of additives (e.g. surfactants) to flowing liquids has been extensively studied since the phenomenon was first observed over 70 years ago. One of the reasons is the huge practical importance of turbulent DR in a wide range of process engineering applications that are commonly found in the food, pharmaceutical, and biomedical industries (Han et al., 2017; Bhambri et al., 2016; Jovanović et al., 2006). Indeed, almost all these applications, such as transport of crude oil in pipelines (Hart, 2014) or heat transfer and exchange (Tiong et al., 2015; Fsadni et al., 2016), involve the use of drag-reducing additives in gas-liquid/liquid-liquid flows.

It has long been argued that DR is determined by the dynamical interactions between additives and turbulence (see Lumley, 1969; Berman, 1978 for further details), yet it was not until recently that progress had been made in

understanding these interactions and predicting DR in turbulent shear flows. Advancements have been granted by the possibility to perform high-fidelity simulations of viscoelastic turbulent flows and detailed measurements of turbulence in dilute/semi-dilute additive solutions, mostly via non-invasive optical techniques. Facing the applications quest for more quantitative information on DR mechanisms, numerical and experimental techniques characterized by unprecedented accuracy and access into the flow have been developed to disclose new features that are peculiar of additive-induced DR phenomena. In this review, we address precisely these phenomena, focusing on the case of polymer- and fiber-induced DR in turbulent wall-bounded shear flows. DR phenomena are discussed in connection with current physical understanding of how polymers and/or fibers interact with the various scales of turbulence: from the small scales resolving the flow in Lagrangian models to the large-scales of Euler-Euler models. Since the targeted field of research is extremely vast, we will cover only the issues relevant to the use of high-molecular weight polymers and fibers as Drag-Reducing Agents (DRA) in processes of industrial interest, leaving other types of additives (surfactants, micro-bubbles and compliant coatings) and applications out of the discussion.

2. Background: Phenomenology of DR

In this section, we will try to highlight current understanding of the microscopic interactions that occur

[†] Received 9 June 2019; Accepted 2 December 2019
J-STAGE Advance published online 29 April 2020

¹ Via delle Scienze 208, 33100 Udine, Italy

² Piazza Garibaldi 18, 33100 Udine, Italy

* Corresponding author: Cristian Marchioli;

E-mail: marchioli@uniud.it

TEL: +39-0432-558006 FAX: +39-0432-558027



between the coherent structures of the flow and the additive, which govern the macroscopic features of DR phenomena. The essential dynamical interactions were poorly understood and remained largely unknown until faithful direct numerical simulations (DNS) of polymer/fiber-induced DR in channel flows became feasible (Kim et al., 2008). We will discuss such interactions considering the review by White and Mungal (2008) as the starting point to provide an update on the advancements that have been achieved over the last decade through numerical and experimental evidence. In their review, White and Mungal (2008) already established that DR produced by polymer and/or fiber additives can be described phenomenologically as the outcome of dynamic interactions that take place between the additive and the turbulent flow. This interaction leads to a significant modification of the near-wall turbulence structure, as demonstrated, for instance, by the LDA measurements of viscoelastic polymer solutions of Escudier et al. (2009), thus altering the nature and strength of the coherent structures that populate this region of the flow and play a crucial role in the self-sustaining mechanism of wall turbulence. The reader is referred to Marchioli and Soldati (2002) and Picciotto et al. (2005), and references therein for further details on these mechanisms. A nice pictorial view of this process, as induced by rigid neutrally-buoyant fibers, was given by Paschkewitz et al. (2004, 2005), and is shown in **Fig. 1**.

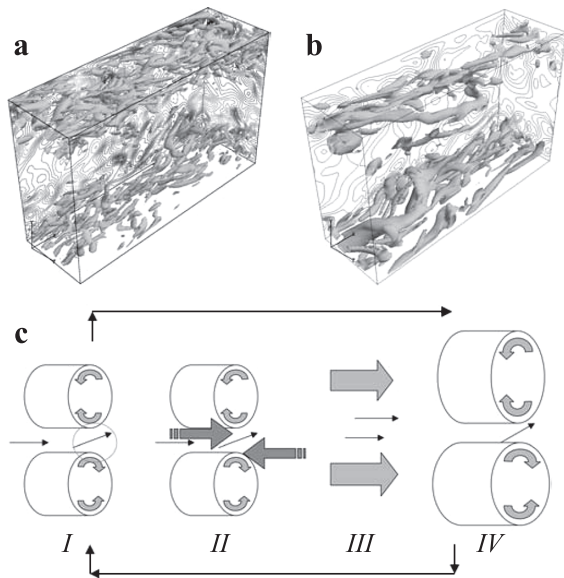


Fig. 1 Instantaneous visualization of near-wall vortices and wall-normal velocity contours for **(a)** single-phase Newtonian and **(b)** fiber-laden channel flow. Fiber parameters: Peclet number $Pe = 1000$, aspect ratio $\lambda = 100$, concentration $nL^3 = 18$. Velocity contours are equally spaced in the range $\pm 0.013U_c$ with U_c the centerline velocity. Panel **(c)**: Mechanism for fiber-induced DR. *I.* Fibers align in inter-vortex regions. *II.* Fibers generate large stresses and body forces that oppose vortex motion. *III.* Vortex structures are dissipated and fibers realign in flow direction. *IV.* Vortices re-emerge and cycle repeats. Reproduced with permission from Paschkewitz et al. (2004).

Panels **(a)** and **(b)** of this figure show the effect of the fibres on the near-wall vortices, which are usually referred to as Quasi-Streamwise Vortices (QSV) and are visualized here using iso-surfaces of the second invariant of the velocity gradient tensor (Blackburn et al., 1996). In the fiber flow, QSVs are both larger and weaker, and the contours of the wall-normal velocity show an increase in spacing. The vortices are also spread out over a larger region in the wall-normal direction relative to the Newtonian flow. In the case of fibers, this happens because fibers that move through the high stress regions of the flow (phase *I* in **Fig. 1**), most pronounced in regions of intense vortex activity, generate large stresses and body forces that oppose to vortex motion (phase *II*). This interaction weakens the vortices and enhances fiber alignment in the flow direction (phase *III*). Upon fiber reorientation, the reduction in local fiber stress allows the vortices to re-emerge and the turbulence is sustained in a weakened state (phase *IV*).

A similar phenomenology is observed in the case of polymer-induced DR, and is summarized in **Fig. 2**, taken from Graham (2014). This figure refers to situations in which the ratio of the elastic forces to the viscous forces within the flow, parameterized by the Weissenberg number Wi (defined more precisely in the next section), are low to moderate. In the case of Newtonian turbulence, the flow is characterized by active intervals, dominated by strong three-dimensional, coherent vortical motions (Marchioli and Soldati, 2002), for the majority of the time and only occasionally enters hibernation intervals. Once Wi exceeds an onset value, indicated as Wi_o in the figure, these flow structures start to stretch the polymer chains. Such stretching weakens the near-wall coherent structures, thus leading to reduction of the friction drag (regarded as the primary mechanism operating at low levels of DR). Specifically, the polymers are stretched within the low-speed streaks and relax as they get rolled into the

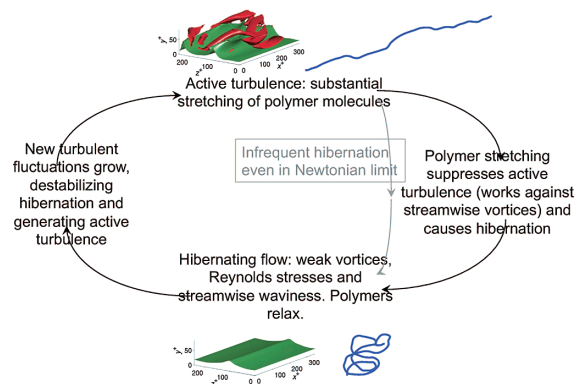


Fig. 2 Schematic of the stochastic cycle displayed by viscoelastic turbulent minimal channel flow at low Reynolds number ($Re \sim 3000$) and moderate Weissenberg number ($Wi \sim 25$). Reproduced with permission from Graham (2014).

streamwise vortices. The resulting polymer force works to loosen the vortices. As Wi further increases, polymer stretching by turbulence becomes persistent and stresses accumulated over time reach: The polymer chain is deformed more rapidly than it can relax, so a threshold value beyond which the active turbulence can no longer sustain itself is reached: Flow hibernation sets in and allows the polymer molecules to relax again. Once the turbulence becomes active again, the cycle repeats. Note that this scenario implies that DR is primarily a near-wall phenomenon. Under these circumstances, a limiting state may be reached, in which turbulence must be entirely suppressed near the wall (Graham, 2014; Wang et al., 2014). The scenario just described is in accordance with several studies (see Paschkewitz et al. (2004), Dubief et al. (2004, 2005) and Gillissen et al. (2008) among others) which revealed that the body forces due to polymeric stresses oppose the vortical motions of the QSV that populate the buffer layer that mediates momentum exchange between the near-wall region and core fluid in channels and pipes.

The similarity between the phenomenological interpretations of Paschkewitz et al. (2004, 2005) and of Graham (2014) highlights the fact that polymer and fiber stress tensors show the same characteristics, at least in the low drag reduction regime as noted by Boelens and Muthukumar (2016). In particular, because fibers cannot store turbulent kinetic energy in their backbone, this mechanism has to be explained by viscosity effects. The macroscopic manifestation of the mechanism just discussed is a reduced wall friction, namely a modified mean velocity profile, a redistribution of the shear stress inside the boundary layer and a reduction in the energy dissipation rate at length scales close to the lower end of the energy cascade yet still within the inertial range (de Chaumont Quiry and Ouellette, 2016; Xi et al., 2013; Ouellette et al., 2009).

Further evidence of the above-mentioned mechanisms has been provided by the analysis of the effect of elasticity on the coherent flow structures, which suggests that the self-sustaining process of wall turbulence becomes weaker because the additive is able to counteract both the biaxial and uniaxial extensional flow regions around QSVs (Roy and Larson, 2006). Above the buffer layer, however, hairpin vortices are more prevalent than QSV. In Newtonian flows, hairpins can regenerate to form hairpin packets that produce large amounts of streamwise kinetic energy, as well as multiple ejections resulting in turbulent bursts and formation of new QSVs (Adrian et al., 2000). Further, hairpin vortex packets significantly contribute to the mean Reynolds shear stress (Jodai and Elsinga, 2016; Ganapathisubramani et al., 2003), which has two parts: the coherent stress caused by non-linear interactions among individual vortices within the packet and incoherent stress originated from velocity fluctuations

induced by each vortex (Lee and Sung, 2011; Adrian et al., 2000). In drag-reduced flows, the hairpins in the log layer are weakened by the counter torques produced by the additive (Kim et al., 2007), similarly to what happens to QSV in the buffer layer. Kim et al. (2008) have examined the time evolution of hairpin packets interacting with a polymer conformation field, showing that the non-linear threshold of initial vortex strength required to trigger auto-generation of new hairpins increases as the flow viscoelasticity increases, especially in the buffer layer. In other words, the generation of new vortices is suppressed by the polymer stresses, thereby decreasing the turbulent drag. Similar findings were obtained by Guan et al. (2013) and Fu et al. (2014). Guan et al. (2013) used time-resolved particle image velocimetry to investigate the effect of DRA on the spatial topological character of coherent vortices in wall-bounded turbulence. Although the (polymer) additive solution was not found to affect the spatial topological shape of these vortices, a drastic decrease of the associated fluctuating velocity and velocity derivatives in the solution was observed. The resulting reduction of the wall friction was ascribed to the suppression of vortex occurrence and intensity. Fu et al. (2014) used particle image velocimetry in combination with planar laser induced fluorescence to investigate DR in turbulent channel flow upon inhomogeneous injection of polymer solution from one channel wall. The focus of the study was polymer diffusion, which controls the local polymer concentration and was found to be suppressed due to turbulence inhibition compared to the diffusion of a passive scalar in unladen turbulence.

Very recently, Elsnab et al. (2019) have provided new experimental evidence of the effect of DR on the structure of turbulence in channel flow. These authors have shown that, for the DR between 6.5 % and 26 %, several fluid velocity statistics (e.g. the mean profile slope in the inertial sublayer or the peak value and peak position of the streamwise r.m.s.) tend to increase with DR in a continuous and essentially linear manner, whereas the relationship between the injected polymer concentration and the level of DR is nonlinear. According to Elsnab et al. (2019), a primary effect of polymer is that it limits near-wall vorticity stretching and reorientation, and thus attenuates/delays the three-dimensionalization of the vorticity field. This scenario is corroborated by the observed onset of the inertial layer at large-enough wall distance, as well as an increase in the scale of the organized vortical motions, and, finally, a reduction in the overall scale separation in the inertial range.

3. Onset of DR, maximum DR and available theoretical frameworks

Two features of DR due to additives have been considered extensively in archival literature: the onset of DR and the so-called Maximum Drag Reduction (MDR) asymptote. In this section, we will recall these features showing how the physical mechanisms of DR and the underlying dynamical interactions between additives and turbulence have been incorporated in suitable criteria to predict DR.

Scaling arguments and experimental data have led to devise a time criterion for polymer-induced DR in wall-bounded flows (Hershey and Zakin, 1967; Lumley and Kubo, 1985), which requires that for DR to occur, the polymer relaxation time must be longer than a representative time scale of the near-wall turbulence, i.e., $T_z > \frac{\mu_s}{\rho_s u_\tau^2}$, where T_z is the average time taken by a stretched polymer to return to a coiled configuration, μ_s and ρ_s are the viscosity and the density of the solution, and $u_\tau = \sqrt{\tau_w / \rho_s}$ is the wall friction velocity, with τ_w the wall shear stress. For a flexible linear polymer in solution, the relaxation time can be expressed as $T_z \sim \frac{\mu_s (N^{3/5} a)^3}{k_B T}$, where N is the number of repeating monomers in the polymer molecule, a is length of a single monomer (the repeat unit from which a polymer is built), k_B is the Boltzmann constant, and T is the solution temperature (Flory, 1953). According to the classical formulation of the time criterion, onset of DR occurs when the ratio of the polymer timescale to the timescale of the near-wall turbulence, defined as the wall-shear Weissenberg number $Wi_\tau = \frac{T_z \rho_s u_\tau^2}{\mu_s}$, is of order unity.

Whenever this condition is met, the polymer molecule undergoes the so-called coil-stretch transition (Somani et al., 2010): Molecules become abruptly stretched and the elongational viscosity increases, up to several orders of magnitude. Elongational viscosity increases preferentially near the wall, where the extensional strain rates are the highest, and acts to suppress turbulent fluctuations, increase the buffer layer thickness and eventually reduce wall friction (Sher and Hetsroni, 2008). The flow-induced coil-stretch transition of high molecular weight polymers has generally been considered to be of first order (Ghosal and Cherayil, 2018). However, there is evidence of significant slowing down in the rate at which the polymers relax to equilibrium in the vicinity of the transition: This suggests that the transition may be more complex, since the slowing down effect is typical of a second-order transition, and characterized by a broad spectrum of conformational states (Ghosal and Cherayil, 2018).

A recent development of the time criterion for DR has been put forth by Boelens and Muthukumar (2016), who investigated numerically the drag-reducing mechanism in the onset regime for both flexible polymers and rigid fi-

bers. Based on the similarity of the polymer and fiber stress tensors in turbulent flow, these authors infer that a common drag-reducing mechanism exists, and suggest that it must be associated with a viscous effect. In particular, they find that all terms in the stress tensor are negligible, except the off-diagonal terms associated with rotation: Therefore, DR arises from rotational motion of fibers and partially stretched flexible chains. Based on these observations, the rotational orientation time is proposed as the unifying time scale to characterize DR by both types of additive. This time scale can be defined as $\tau_r = K V_f \mu_s / k_B T$, where K is a proportionality constant including terms related to the shape and the volume of the rotating molecule, and V_f is the free space per molecule. The rotational orientation time of rod-like macromolecules can be obtained either directly by dielectric measurements or by relaxation of dichroism, or indirectly by viscoelastic measurements (Boelens and Muthukumar, 2016).

The time criterion for DR is generally confirmed by numerical and experimental data, yet the omission of polymer concentration represents a serious limit to the application of the criterion for predictive purposes. Indeed, several works in which mono-disperse polymers characterized by a single value of T_z (instead of a distribution of T_z as found for poly-disperse polymers) have demonstrated that the onset of DR depends systematically on polymer type and concentration (Campolo et al., 2015; Yang and Ding, 2013). The contribution of concentration in determining the onset of DR has been accounted for in the context of the so-called elastic theory developed by De Gennes and co-workers (Tabor and De Gennes, 1986; de Gennes, 1990) based on the elastic behaviour of stretched polymers. According to this theory, DR by coil-stretch transition occurs when the elastic energy stored by the partially-stretched polymers, which increases with decreasing length scale of turbulence (i.e. increased stretching characteristic of turbulence dynamics), becomes comparable to the energy of the turbulent flow, which decreases with the scale size. When this situation occurs, the elastic energy interferes with the turbulent cascade mechanism preventing it to proceed all the way to the Kolmogorov scale (Xi et al., 2013). This can lead to buffer layer thickening and reduced drag. Experimental measurements by Ouellette et al. (2009, 2016), who studied the effect of long-chain polymers on the Eulerian structure functions in a turbulent von Kármán swirling flow, support this framework as they indicate that the introduction of polymers into the flow modifies the energy cascade by extracting turbulent kinetic energy from the flow and partially dissipating it directly (Valente et al., 2014). As a result, the rates of energy injection, transfer and dissipation for the turbulence are no longer all equal, as they must be in Newtonian turbulence where viscosity provides the only mechanism of energy dissipation.

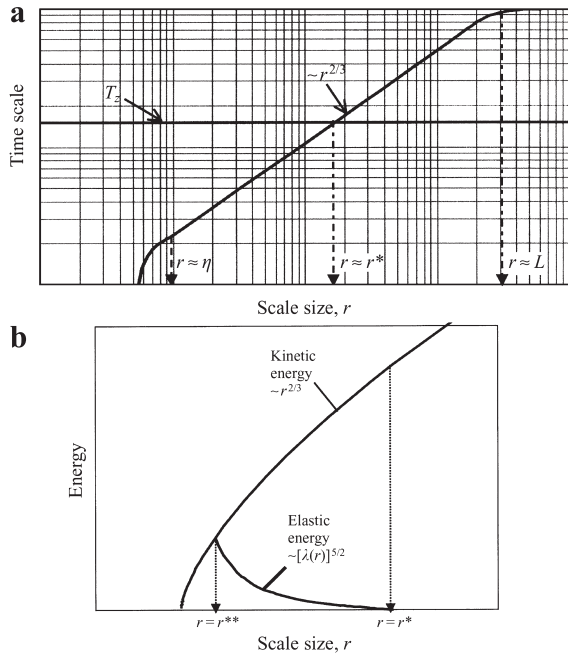


Fig. 3 Schematic representation of the elastic theory for the onset of DR. Panel (a) shows the time scales in homogeneous turbulence, including the onset length scale r^* . The 2/3 power law is valid for scales larger than the Kolmogorov scale η , L being the largest flow scale. Panel (b) sketches the condition for which the scale r^{**} can be determined, namely when the turbulent energy per unit volume, which scales as $r^{2/3}$, is equal to the elastic energy per unit volume, which begins to grow at r^* and scales as $[\lambda(r)]^{5/2}$, with $\lambda(r) = (r^*/r)^\alpha$ the power law of polymer stretching for $r < r^*$. Reproduced with permission from Sreenivasan and White (2000).

When the elastic theory is applied to homogeneous isotropic turbulence, one might expect that, for a given combination of the polymer and the flow and using the same notation as in Sreenivasan and White (2000), a turbulent length scale r^* exists, whose corresponding time scale τ_r^* matches T_Z , as sketched in **Fig. 3(a)**. This length scale can be expressed as $r^* = u_{r^*} T_Z$, with u_{r^*} the velocity scale characteristic of the scale r^* . Following Kolmogorov 41 theory, such velocity scale can be expressed as $u_{r^*} = (r^* \langle \epsilon \rangle)^{1/3}$. Polymer molecules are expected to undergo stretching by all scales smaller than r^* and to affect the flow only at scales smaller than r^{**} . The scale r^{**} is smaller than r^* and can be determined assuming that the elastic energy per unit volume stored by the polymer equals the turbulent energy per unit volume that can be associated to that scale, as sketched in **Fig. 3(b)**. Another crucial result of the elastic theory is the relation that connects the elastic energy with the power law scaling of polymer stretching, which reads as $G[\lambda(r^{**})]^{5/2} = \rho_s u_{r^{**}}^2 = \rho_s (\epsilon_T r^{**})^{2/3}$ (Sreenivasan and White, 2000), where $G = ckT/N$ is the elastic energy (c being the polymer concentration in units of monomers per unit volume) and the quantity on the right-end side is the turbulent kinetic energy at scale r^{**} , which can be expressed via the energy

transfer rate per unit mass through the inertial range, ϵ_T . Note that, in non-Newtonian turbulence, ϵ_T differs from the energy injection rate through the cascade and from the energy dissipation rate due to viscosity, since polymers can provide a non-viscous mechanism for draining energy from the cascade (de Chaumont Quitry and Ouellette, 2016). When concentration is very small, the scale r^{**} will be smaller than the Kolmogorov scale η and the turbulence will be unaffected by the polymer. A minimum concentration exists for which $r^{**} = \eta$, and onset of DR occurs. Following the onset, for a fixed value of the flow Reynolds number Re , DR initially increases with polymer concentration but saturates beyond a certain value. This threshold value for concentration corresponds to the so-called Maximum Drag Reduction (MDR), which is generally attributed to the dynamics being reduced to a marginal yet persistent state of subdued turbulent motion (Virk, 1975; Li et al., 2015; Choueiri et al., 2018). In the literature, the MDR asymptote is found to be identical for different types of polymer-solvent combinations (Calzetta, 2010). For a fixed value of polymer concentration, DR initially increases with increasing Re , following a unique concentration-dependent trajectory up to a certain Re after which an abrupt change of trajectory is observed. Such change indicates the location at which the DR curve merges with the MDR asymptote.

One scenario is that MDR occurs when the concentration of the polymer is high enough to allow for unstretched coils to overlap. This implies (see also Sreenivasan and White (2000) for experimental validation) that $G_m = \rho_s u_\tau^2 \cdot Wi^{-1}$ where G_m is the elastic energy when concentration is equal to the value c_m at which DR data cross over the MDR asymptote. Since this expression for G_m neglects the dependence on the scale r^{**} , the following additional expression for the energy can be derived (Sreenivasan and White, 2000):

$$\left[\frac{G_m}{\rho_s u_\tau^2} \right]^{1/3} Wi^{5/6} = Re_\tau^\beta, \quad (1)$$

where $Re_\tau = u_\tau R/\nu$ is the shear Reynolds number of the flow (R being the characteristic size of the flow domain, e.g. the pipe radius in pipe flow) and β is a constant that can be determined upon comparison with experiments. For pipe flow, the best agreement with available data is obtained for $\beta \simeq 1$, which implies that r^{**} near the MDR asymptote scales with R . The interpretation of this scaling is that, at the MDR asymptote, a small amount of stretching (characteristic of length scales of order R) will be enough to make the elastic energy of the polymer comparable to the turbulent kinetic energy of the fluid. When this condition is met, polymers cause the growth of the buffer layer thickness across the entire boundary layer.

In spite of the apparently sound theoretical ground on which the theory is based, and despite the agreement with

several experimental datasets, the phenomenological explanation just discussed is not able to provide a unique bounding mechanism of MDR. First off, the theory is not self-consistent since it assumes that, whenever stretched, polymers can drain energy from the flow but also that they can affect the flow only at scales $r < r^{**} < r^*$. This inconsistency was addressed by Xi et al. (2013), who proposed to modify the original elastic theory framework by balancing the rate of energy transfer rather than the energy itself. By doing so, these authors were able to identify the scale at which the additive is expected to affect the energy cascade and use this scale to collapse their experimental DR data on a single master curve. The same model, referred to as energy flux-balance model, has been assessed by de Chaumont Quirly and Ouellette (2016), who focused on the characterization of concentration effects on the Eulerian and Lagrangian structure functions. One example of their results is provided in **Fig. 4**, which shows the compensated velocity transverse structure function, D_{NN} , expressed as:

$$\left[\frac{3}{4} \frac{D_{NN}(r)}{C_2 r^{2/3}} \right]^{3/2} = \epsilon_T, \quad (2)$$

where C_2 is a known scaling constant. The figure compares the compensated structure function for pure water with that obtained for polymer solution at varying concentration ϕ , expressed in ppm, at high Re but moderate Wi . As ϕ increases, the structure function reaches a plateau at larger length scales and the value of this plateau is different from that measured in pure water. The important points, however, are that (1) data for different polymer concentrations are found to collapse when curves are rescaled by the factor $\phi^{2/5}$ (see Xi et al. (2013) for further details), and (2) data collapse on two distinct curves: One for concentrations below 5 ppm and one for concentrations above 10 ppm. Such different ϕ -dependent behaviour was ascribed to the possible onset of interactions between individual polymer chains, which are favoured at higher concentrations and are more likely at small Wi (e.g. below the range for which a sharp coil-stretch transition is observed). Based on these findings, which were observed to hold also for structure functions in the time domain, de Chaumont Quirly and Ouellette (2016) concluded that the energy flux-balance model seems to be able to capture the essential effect of polymer concentration on turbulence, even if its application should be limited to dilute solutions.

In addition, there is evidence of situations in which MDR occurs when the Reynolds stresses are due primarily to the fluctuating stresses of the additive (see White and Mungal, 2008 for further details) and situations in which the polymer concentration field is inhomogeneous, e.g. in injection experiments: The theory does not take such inhomogeneities into account. Most importantly, however, the difficulty in predicting MDR comes from the fact that the flow, at the onset of MDR, does not reach a purely laminar state: Rather, turbulence is reduced (either via elastic or viscous effects or both) to a marginal state at the edge between laminar and turbulent motion. This may suggest the existence of a peculiar self-sustaining transitional flow regime in which the stresses produced by the additive play a key role and promote DR mechanisms that are inherently different from those known for Newtonian fluids. Indeed, very recent results from Choueiri et al. (2018) provide evidence of a dynamical disconnection of the asymptotic state from ordinary turbulence: These authors show that, for an appropriate choice of parameters, additives can reduce the drag beyond the MDR limit, eliminating turbulence and giving way to laminar flow. At higher polymer concentrations, however, the laminar state becomes unstable, resulting in a fluctuating flow with the characteristic drag of the MDR asymptote. At sufficiently high Reynolds numbers, such flows are observed to be structurally different from

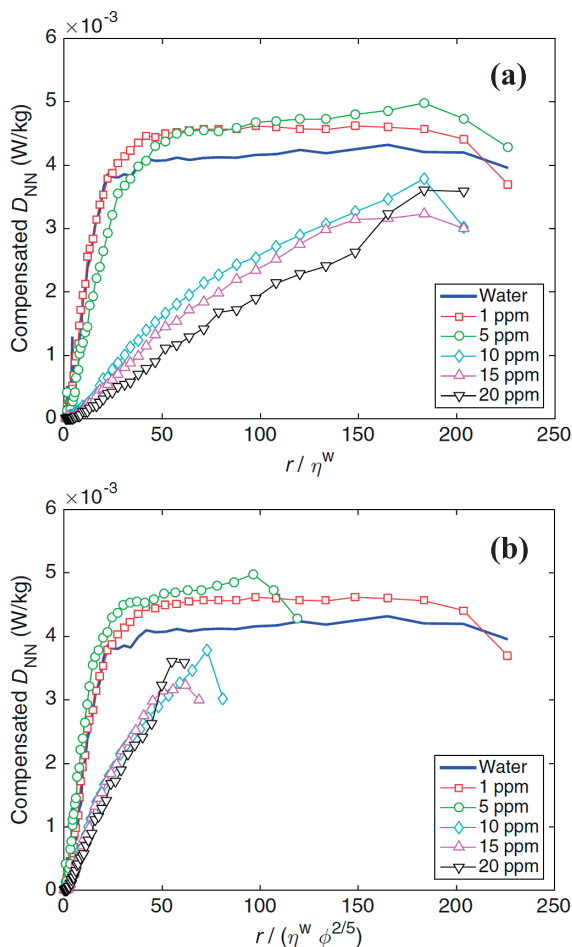


Fig. 4 Panel (a): Compensated transverse velocity structure function as a function of r/η^w , with η^w the Kolmogorov scale in flow of pure water. Panel (b): same data as in panel (a) with length rescaled by a factor $\phi^{2/5}$, derived from the energy flux-balance model. Reproduced with permission from de Chaumont Quirly and Ouellette (2016).

Newtonian turbulence albeit being characterized by streak patterns that are similar to those resulting from elastoinertial turbulence at Reynolds numbers well below the threshold for Newtonian turbulence. This type of behaviour has brought to a new interpretation of MDR, which is based on the idea that the dynamics of the flow upon onset of MDR are driven by the elastoinertial instability for high-enough polymer concentrations (Choueiri et al., 2018; Samanta et al. 2013). In other words, the MDR limit and the characteristic approach towards it may be seen as the result of two states of turbulence: Newtonian turbulence and elastoinertial turbulence. When these two turbulent states coexist, a transition from one to the other is observed. Based on such observations, Choueiri et al. (2018) have proposed a state map for Reynolds number versus polymer concentration, in which the different manifestations of turbulent flow observed for a specific type of additive (polyacrylamide) are summarised. This map is reported in **Fig. 5** and shows a number of interesting features. First, the onset of turbulence (the left lower branch in **Fig. 5**) is delayed by the action of polymers. Second, as Re is increased, turbulence sets in as localized turbulent puffs and, subsequently, to growing turbulent slugs provided that polymer concentration remains below a certain threshold of concentration ($C < 20$ ppm in **Fig. 5**). The onset of puffs and slugs is delayed compared to Newtonian fluids, and leads to mixed state which then eventually approaches MDR instead of allowing for complete relaminarization of the flow. Third, above the threshold for concentration, fluctuations set in more uniformly in space and lack the spatial intermittent character of the Newtonian transition scenario. For a further increase in concentration ($C > 90$ ppm in **Fig. 5**), this instability occurs at Re significantly smaller than the lowest value for which Newtonian turbulence would be observed.

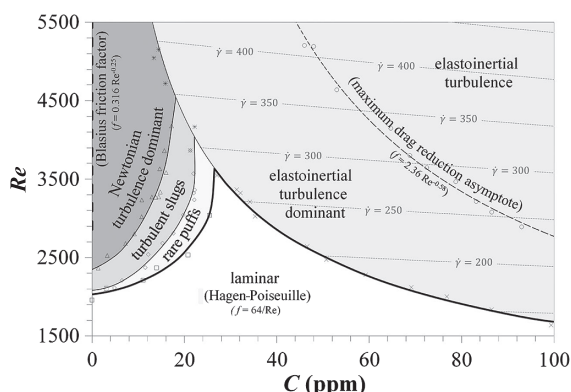


Fig. 5 State map for Reynolds number versus polymer concentration. While Newtonian turbulence is controlled by the Reynolds number, elastoinertial turbulence and its instabilities are controlled by the relation between shear rate $\dot{\gamma}$ and concentration. Iso- $\dot{\gamma}$ lines are shown in the portion of the map where elastoinertial instabilities are observed. Reproduced with permission from Choueiri et al. (2018).

The important finding here is that, at intermediate concentrations, elastoinertial instability sets in before MDR is reached.

The discussion made so far highlights that drag reduction may be characterized by relatively few dimensionless groups, notably the flow Reynolds number and the Weissenberg number. Such parameter space has been nicely summarized by Graham (2014), and the schematic proposed by this author is shown in **Fig. 6**. In this figure, Ex is the extensibility number, representing the maximum value of the ratio between the extensional stress due to the polymer and the extensional stress due to the solvent, $\beta = \mu_s/(\mu_s + \mu_p)$ with μ_s the solvent viscosity and μ_p the additive viscosity, while $El = Wi/Re$ is the elasticity number ($El = 0$ for Newtonian flow). For a given set of experiments, Ex and β have constant value the schematic provides the DR map as a function of Re and Wi only. Each oblique line in the figure is characterized by constant El and represents a series of experiments at increasing flow rate. As Re increases, transition from laminar to turbulent flow occurs. The lowest oblique line, labeled “A”, corresponds to small El . As flow rate increases, transition to turbulence occurs first, then at some higher flow rate, Wi becomes sufficiently large for the polymers to stretch and DR to set in. This onset Weissenberg number, denoted as Wi_0 in the figure, is around 10–20. The MDR regime is eventually reached at Re much higher than those considered in the plot. The line labeled “B” corresponds to larger El , and refers to a situation in which transition occurs at a sufficiently high Wi to prevent Newtonian turbulence: Polymer relaxation is slow enough to leave the turbulence unaffected by viscoelasticity, yet the flow rate must still increase beyond transition to reach MDR. The line labeled “C” corresponds to values of El large enough to let the flow enter the MDR regime directly upon transition to turbulence. Finally, the line labeled “D” corresponds to the case of elastoinertial turbulence (referred to

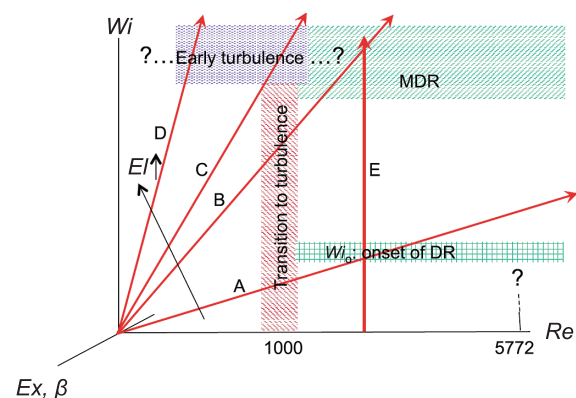


Fig. 6 Parameter space of turbulence and DR in dilute polymer solutions. Boundaries are in general fuzzy and oblique. The linear stability limit $Re = 5772$ is also shown but is not relevant for the present discussion. Reproduced with permission from Graham (2014).

as early turbulence): In this case, transition can occur at significantly lower Re than in Newtonian flow. As mentioned by Graham (2014), the detailed correspondence between this regime and the MDR regime is still poorly understood. Experiments suggest the existence of a continuous transition from the laminar flow curve to the MDR curve, driven by the occurrence of some kind of linear instability of the laminar state at sufficiently high Re and El : To the best of our knowledge, however, no simulation data obtained from available viscoelastic constitutive models has provided evidence of such linear instability yet.

4. Recent analyses of DR onset and MDR in wall-bounded turbulence

In this section, we provide a survey of both numerical and experimental analyses of DR onset and MDR in wall-bounded flows, with a twist towards viscoelastic effects, to highlight current trends and research pathlines in the study of turbulence-additives interaction. Shahmardi et al. (2019) investigated the turbulent flow of a polymer solution in non-axisymmetric square ducts, using the FENE-P model to simulate the presence of polymers. The main macroscopic effect associated to the presence of the polymers is to modify the secondary flow by increasing the circulation of the streamwise main vortices and moving the location of the maximum vorticity towards the centre of the duct. In addition, the low- and high-speed streaks that characterize the fluid velocity distribution near the wall are found to grow in size and coherence. As far as the viscoelastic behaviour of the flow is concerned, the Weissenberg number is found to influence strongly the flow (as also shown in Zhou and Schroeder, 2016): The cross-stream vortical structures grow in size and the in-plane velocity fluctuations are reduced as flow elasticity increases. Overall, the viscoelastic flow is less uniform than its Newtonian counterpart, even if the direct contribution of the polymer stress term in the energy budget is found to be small in amplitude. The same type of numerical approach, namely direct numerical simulation of an incompressible FENE-P fluid, was employed by Li et al. (2015) and Teng et al. (2018) to study DR in both turbulent Poiseuille and Couette flow in a plane channel. Focus of the analysis was the additive-induced modification of the near-wall flow structures. In Poiseuille flow, the ratio of polymer relaxation time to the time scale of vorticity fluctuations in the mean flow direction is found to remain close to unity in the near-wall region, from the onset of DR to MDR. Moreover, the average axial energetic vortex convection time is observed to increase with increasing DR while its rotation speed decreases. Since the rate of decrease in the rotation speed is found to exceed the in-

crease of the vortex convective time, MDR is achieved when these two time scales become nearly equal. A similar DR mechanism is observed in Couette flow only in the near-wall region. In the core region of the flow, differences are found, the most intriguing being the significant polymer stretching that arises from a more intense mutual exchange between the elastic potential energy and the turbulent kinetic energy of the flow (Teng et al., 2018). Also, the spanwise and wall-normal components of the conformation tensor are found to reach their peak value: Such finding is in contrast with that observed in Poiseuille flow, where polymer stretching and elastic/kinetic energy exchanges in the core region are negligible and peak values of the conformation tensor components occur near the wall (Teng et al., 2018).

White et al. (2018) also investigated polymer drag-reduced flow in a wall-bounded domain, focusing on the redistribution of mean momentum and the mechanisms underlying the redistribution processes in channel flow. From a mechanistic perspective, the experimental observations of White et al. (2018) indicate that polymers reduce the intensity of near-wall vorticity stretching, thus leading to an outward migration of the peak in the Reynolds shear stress and its gradient. In turn, such migration leads to a reduced mean velocity gradient at the wall, a more gradual decay of the mean vorticity, and causes the wall-normal position where inertially dominated mean dynamics occurs to move outward from the wall. At high enough DR, the inertial sublayer runs out of physical space and ceases to exist: This implies that the state of MDR is attained only upon annihilation of the inertial sublayer.

Owolabi et al. (2017) investigated experimentally the turbulent DR mechanism in flow through ducts of circular, rectangular and square cross-sections using two grades of polyacrylamide (a flexible linear polymer) in aqueous solution having different molecular weights and various semi-dilute concentrations. The authors explored the relationship between DR and fluid elasticity, exploiting the polymer mechanical degradation¹ to vary the rheological properties of the solution. Under controlled degradation conditions, streamwise velocity profiles at various levels of DR indicated a thickening of the buffer layer, up to the entire cross-section at MDR, in agreement with previous studies (Gillissen and Hoving, 2012; Paschkewitz et al., 2004). Based on their measurements, Owolabi et al. (2017) were able to derive a quantitative prediction of DR from the knowledge of polymer relaxation time, flow rate and geometric length scale (using either the Newtonian pressure drop combined with rheology data, or the average shear rate as an initial guess to

¹Mechanical degradation and its effects on DR will be discussed in Sections 5 and 6.

determine Wi , combined with an iterative procedure). This prediction reads as:

$$DR\% = 2C_\infty \left(\frac{1}{1 + \exp(Wi_c - Wi)} - Wi_c \right) \quad (3)$$

with C_∞ the approximate limiting value of $DR\%$ as $Wi \rightarrow \infty$ and Wi_c the critical Weissenberg number for the onset of drag reduction (set to be $Wi_c = 0.5$, in agreement with the theory of Lumley, 1973). In observing a working functional dependence of $DR\%$ on Wi alone, the depen-

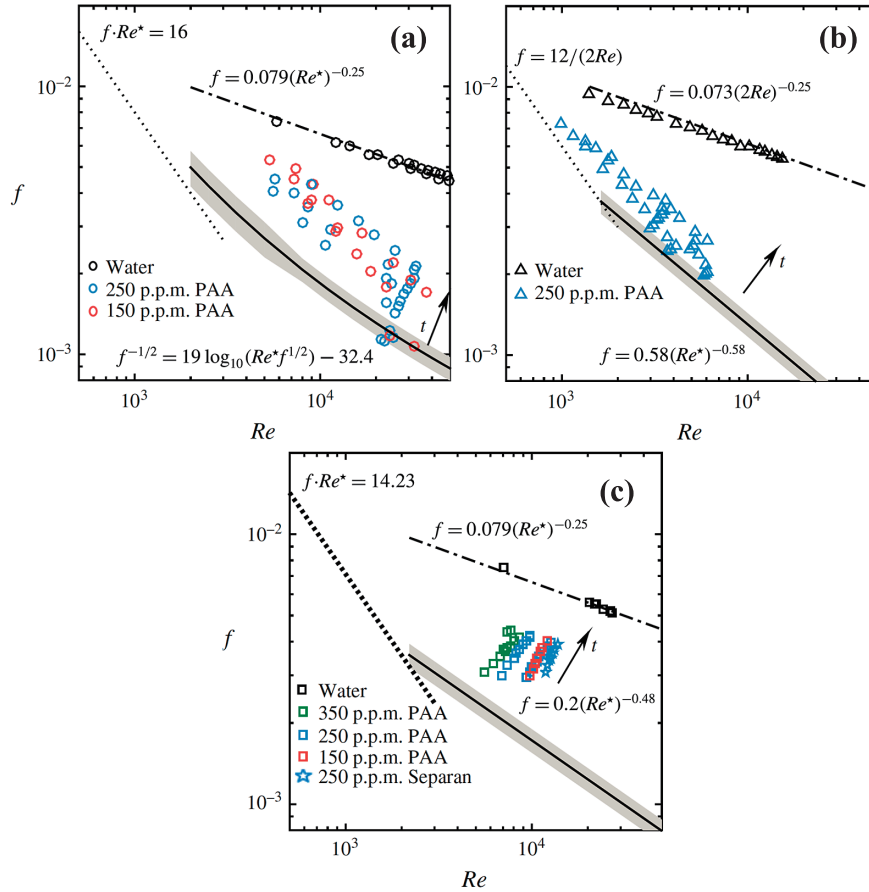


Fig. 7 Fanning friction factors at different flow rates and pumping times for (a) pipe, (b) rectangular channel and (c) square duct. Dotted lines represent the appropriate laminar flow equations for Fanning friction factor; dot-dashed lines represent the correlations of Blasius for pipe and square duct and of Dean for rectangular channel; solid lines represent the correlations of Virk (1975) for pipe and rectangular channel and of Hartnett et al. (1986) for square duct at MDR; the shaded regions represent $f = \pm 10\%$ of MDR. Reproduced with permission from Owolabi et al. (2017).

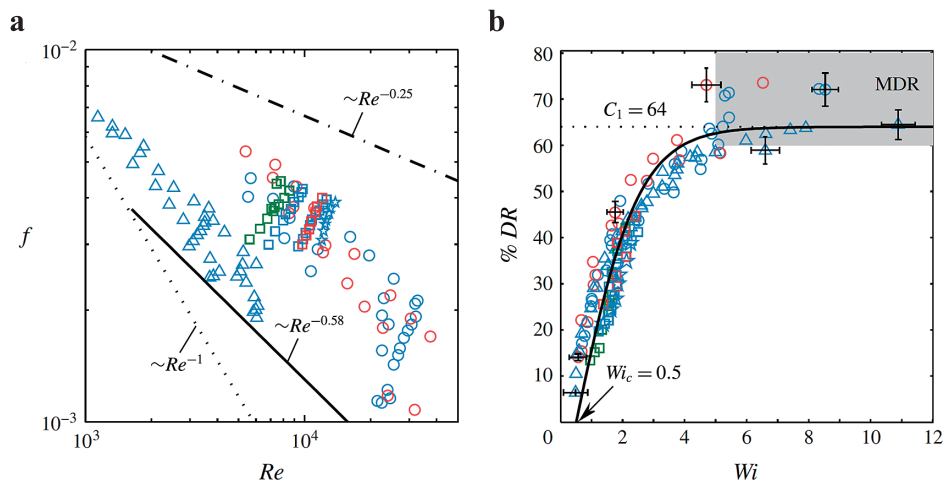


Fig. 8 (a) Combined $f-Re$ data for cylindrical pipe, rectangular channel and square duct (symbols and colours as in Fig. 7). (b) Variation of $DR\%$ with Weissenberg number. The solid black line represents Eq. 3. Reproduced with permission from Owolabi et al. (2017).

dence on the ratio β of solvent to total viscosity, on inertia (i.e. on the flow Reynolds number) and on other viscometric functions, e.g. first or second normal-stress differences, is neglected. In spite of these approximations, the prediction fits reasonably well with the data, as shown in **Figs. 7** and **8**. It must be noted that, in the MDR limit, some weak Reynolds number dependence remains, as $DR\%$ scales roughly as $Re^{0.1}$ in this limit, and there is a spread in the literature for data nominally at MDR (Graham, 2014), highlighted by the grey region in **Fig. 8(b)**. Given the quality of the data collapse illustrated in **Fig. 8(b)**, however, the authors concluded that both β and Re should be regarded as second-order effects, at least for the concentrations and range of Re investigated.

Another correlation to predict the upper limit of DR using polymers as DRA has been proposed recently by Zhang et al. (2018), for the case of turbulent pipe flow. The main equation of the model computes the average drag reduction as:

$$DR\% = (1 - \beta) \left(1 + \frac{1}{12Wi^2} \right) \cdot \mathcal{H} \quad (4)$$

where β is the ratio of the solvent viscosity to the liquid viscosity after the polymer is added at the zero shear rate, and $\mathcal{H} = \frac{1-c-l^2}{(1-c/l^2)^3}$, with c the trace of the conformation tensor and l the dimensionless maximum length of the polymer in the solution. Since c and l cannot be measured, the above equation must be used assuming $c = 0$ to make it useful for practical engineering applications. The model assumes that all vortex structures disappear in the turbulent flow, i.e. complete laminarization is achieved. A slightly older work on DR in dilute polymer solutions was carried out by Xi and Bai (2016). These authors investigated the laminar-turbulent transition of the solution showing its connection with MDR. The idea of the study comes from the speculation (prompted by the universality of MDR) that the MDR asymptote might be associated with a class of weak or marginal turbulent states that already exist in Newtonian flows but only become unmasked at high levels of polymer elasticity. As fluid elasticity increases, the transition to hibernating states becomes much more frequent, resulting in them taking up a larger proportion of the overall statistics or a flow more dominated by features of MDR. This idea clearly hints to the already-mentioned DNS results (Graham, 2014; Xi and Graham, 2012) on the intermittent transitions between strong active turbulence and weak hibernating turbulence. Xi and Bai (2016) identified the marginal state associated to the weakest form of turbulence that can be sustained as a dynamical edge state consisting of traveling waves and relative periodic orbits. The dynamics of such state are characterized by low-frequency fluctuations and exhibit regular bursts of turbulent activities separated

by extended quiescent periods. The flow field is dominated by elongated vortices and streaks, with weak extensional and rotational motions. Flow structures and ES kinematics match hibernating turbulence and, according to Xi and Bai (2016), offer explanations for the existence and universality of MDR. Yet, the quantitative magnitude of MDR still remains unsolved.

Fujimura et al. (2017) studied numerically the influence of the polymer aggregation length on turbulent DR in channel flow. Polymer aggregation was modeled using a bead-spring chain model. The authors find that the local polymer relaxation time increases as the natural length of the polymer increases and the spring constant decreases, and observe that DR increases logarithmically with the relaxation time. Based on this logarithmic dependency, the authors speculate that the drag-reducing effect of the polymer occurs when it is longer than the diameter of turbulent vortical structures: Longer polymers are found to induce higher energy dissipation upon interacting with the flow structures and tend to suppress turbulent fluctuations. The role of polymer length was also examined by Yang and Dou (2010) in connection with wall roughness effects. These authors proposed and validated a theoretical formula to describe the flow resistance in laminar, transitional and turbulent flows from the hydraulically smooth regime to the fully rough one. This formula was developed based on the findings that, while polymers in smooth pipe flow increase the viscous sublayer thickness (thus leading to DR), polymers in rough pipes also increase the near-wall velocity when compared to Newtonian flow conditions, implying that roughness has a negative effect on DR. Indeed, larger roughness tends to narrow the gap between the resistance in viscoelastic flows and that in unladen flows.

As far as analysis of fiber-induced DR is concerned, Moosaie and Manhart (2011, 2013) used a sophisticated rheological model based on direct Monte-Carlo solver to compute fiber orientation dynamics and study the effect of Brownian diffusivity and fiber aspect ratio on the non-Newtonian stress generated by the fibers. The model enables stochastic simulation of the Fokker-Planck equation, in contrast to the moment approximation simulation approach used by Paschkewitz et al. (2004), which requires a closure model. Application of the model to turbulent channel flow shows a shift of the logarithmic law region of the mean velocity profile, indicating a thickening of the viscous sublayer. The streamwise velocity fluctuations are enhanced, while the spanwise and wall-normal ones are attenuated. However, there are discrepancies with the results of the moment approximation approach. The closure model required by the moment approximation approach provides wrong estimates of the mean non-Newtonian shear stress at the wall: This has a direct effect on the wall stress deficit and hence on the

amount of DR (Moosaie and Manhart, 2013).

Fiber-induced DR has been investigated also by Gillissen and Hoving (2012). These authors performed pipe flow experiments showing that turbulent DR in plug-flow of concentrated suspensions of macroscopic fibers is a self-similar function of the wall shear stress over the fiber network yield stress. This behaviour was modelled in terms of a central fiber network plug, whose radius is determined by the yield stress. The pipe cross section can then be divided into a solid plug for $r < r_c$, with r_c the radial coordinate at which the surface of the plug is located (corresponding to the point in the pipe where the shear stress of the fluid equals the fiber network yield stress), and a Newtonian annulus for $r > r_c$. The plug constrains the size of the turbulent eddies in the surrounding annulus, thus reducing the friction factor as compared to Newtonian flow. Note that, if the notion that a large aspect ratio is key for DR, then one should expect polymers and fibers to reduce the drag by similar mechanisms. The experiments by Gillissen and Hoving (2012), however, showed marked differences, e.g. in the profiles of the mean flow. Polymers act in the near-wall, buffer layer, effectively thickening the viscous sublayer, while leaving the momentum transfer in the turbulent core unaffected. Macroscopic fibers, on the other hand, act in the turbulent core, and have little effect in the near-wall region. This difference stems from the different lengths of polymers and fibers. Polymers are usually of sub-Kolmogorov length scale and, on the scale of the near-wall vortices, can be regarded as a continuum that induces an additional viscosity and acts to reduce the momentum transfer of the near-wall vortices (Voth and Soldati, 2017). Fibers, on the other hand, are rarely below the Kolmogorov scale. Rather, they are usually orders of magnitude larger than the near-wall vortices and, instead of inducing internal friction, tend to impose external constraints on the near-wall vortices, which are thus forced to restructure themselves.

5. Predictive correlations for DR in wall-bounded flows

In the previous sections, we focused on the phenomenology of polymer/fiber-induced turbulent DR and on the theoretical frameworks that have been developed to explain the underlying physics. In this section, we focus on one aspect of practical relevance for the design of industrial systems exploiting DRA, namely the predictive correlations that are available to determine amount of DR expected for a given DRA concentration in a specific solvent. The amount of DR can be predicted using two types of correlations: those that simply fit the experimental data (typically collected in small-scale pipes), whose predict-

ability for industrial scale applications is however rather limited (Campolo et al., 2015), or those developed based on physics of the DR phenomena which appear more promising in the industrial practice (Dubief et al., 2005). Given the wealth of correlations for drag-reducing flows that are available in the literature, we will purposely focus only on those providing the friction factor. Specifically, we will discuss results from unpublished experimental tests made with polymers (polyethylene oxide, PEO) in pipes of different diameter, equipped with centrifugal pumps to assess the predictive capability of some widely-used correlations, discussing the efficacy of the tested additives as DRA. Tests were performed under controlled conditions: A pre-mixed homogeneous mixture of additive and solvent was introduced in the test rig and pumped along the loop using a low-shear pumping system in order to avoid peaks of shear stress, which could prematurely degrade the additive (Elbing et al., 2009; Choi et al., 2000). Details on the experimental facility are provided in Campolo et al. (2015).

The theoretical variation of friction factor expected in the polymeric regime when polymer degradation is negligible reads as (Shetty and Solomon, 2009; Virk, 1975):

$$\frac{1}{\sqrt{f}} = (4 + \delta) \log_{10}(Re\sqrt{f}) - 0.4 - \delta \log_{10}(Re\sqrt{f})^* \quad (5)$$

where δ is the slope increment and $(Re\sqrt{f})^*$ is the onset Reynolds number, defined as:

$$(Re\sqrt{f})^* = \frac{\sqrt{2\tau_w / \rho} \cdot D}{\nu_s} \propto \tau_w^{0.5} \propto \gamma_w^{0.5} \quad (6)$$

where D is the pipe diameter, ν_s is the kinematic viscosity of the solvent, τ_w is the wall shear stress and γ_w is the wall shear rate. **Fig. 9** shows the results of tests performed in the pipes using PEO (Polyox WSR-301 by Dow Chemicals), and hydrolized Polyacrylamide (HPAM, Magnafloc 1011 by Basf) as water-soluble polymer. Each panel in the figure shows the variation of friction factor, $1/\sqrt{f}$, for a given polymer concentration (symbol) as a function of wall Reynolds number, $Re\sqrt{f} = Re_\tau\sqrt{2}$, in Prandtl Karman coordinates. The black line represents the Prandtl-Karman friction factor (P-K) for pure water and smooth pipe; the gray line in the top left corner represents Virk's MDR asymptote. Dashed lines shown together with the experimental points represent the theoretical variation of friction factor given by Eq. (5). The experimental data follow the polymeric regime up to a threshold value of $(Re\sqrt{f})^*$ above which they depart from theory due to mechanical degradation. The latter can be ascribed to two different phenomena: the mechanical degradation due to turbulence and the mechanical degradation due to the injection system. Mechanical degradation due to turbulence is associated to breakage of the monomers of the polymer chain produced when the shear

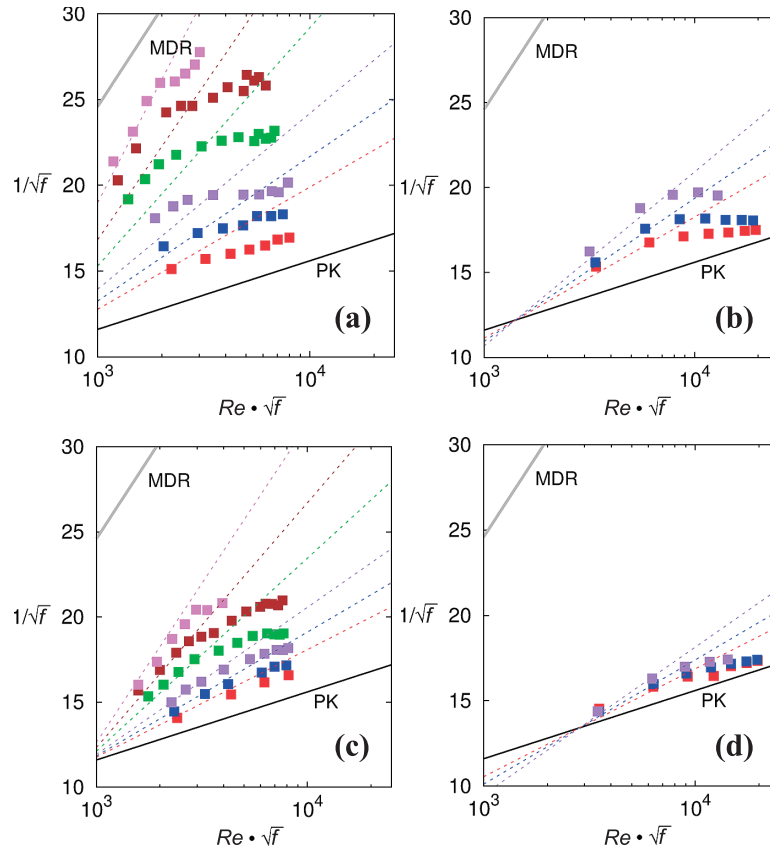


Fig. 9 Prandtl-Karman plot of friction factor variation produced by polymer injection: different symbols refer to different polymer concentrations; each row shows the effect of polymer type: WSR-301 (top row) and Magnafloc 1011 (bottom row); each column shows the effect of pipe diameter ($D = 30$ mm, left column; $D = 100$ mm, right column); colours represent concentration (0.25 ppm, red; 0.50 ppm, blue, 1.00 ppm violet; 2.50 ppm, green; 5.00 ppm, brown; 10.00 ppm, purple). Results from the Authors.

rate exceeds the threshold value γ_w^* which is a function of polymer molecular weight, M_w : $\gamma_w^* = A \cdot M_w^B$, with A and B coefficients that depend on polymer type (Elbing et al., 2009). For PEO: $A = 3.4 \cdot 10^{18}$ and $B = -2.20$; for HPAM: $A = 1.16 \cdot 10^{23}$ and $B = -2.73$. We remark here that, following Tabor and De Gennes (1986), the onset condition identifies a value of the fluid time scale, usually equal to $1/\gamma_w$, matching the relaxation time scale of the polymer, which depends on the polymer molecular weight. This yields $\gamma_w \propto M_w^{-1}$. The use of such relation assumes that the onset of drag reduction is independent of polymer concentration. This assumption has been widely used since Virk (1975) showed a negligible influence over a wide range of polymer concentrations. However, other studies (see Elbing et al. (2009) and references therein) have shown that weak concentration dependence may be observed under certain conditions. Winkel et al. (2009) and Vanapalli et al. (2006) found that $\gamma_w = a \cdot M_w^{-1}$ with $a = 3.35 \cdot 10^9$ for PEO, as derived from the experimental data reported by Campolo et al. (2015). Elbing et al. (2009) report $\tau_w = 1.68 \pm 0.60 Pa$ for HPAM having $M_w = 5.5 \cdot 10^6$ from which one can calculate $a = 9.25 \cdot 10^9$. The slope increment δ depends on molecular weight and concentration, whereas it should not depend on pipe di-

ameter (Campolo et al., 2015) and a specific slope increment $\delta/C^{0.5}$ can be defined to characterize the drag reducing ability of a polymer-solvent pair and an intrinsic slope increment $\Pi = \delta/(C/M_w)^{0.5}$ can be defined which depends only on the species skeletal structure. Based on these assumptions, one can use experimental data to identify the value of onset Reynolds number and slope increments.

The second mechanism for polymer chain degradation is due to the injection system, characterized by locally large values of strain rate, $\dot{\epsilon}_D = u_{ss}/d$, with u_{ss} and d the velocity of polymer master solution and the injection pipe diameter, respectively. Recent experimental evidence (Elbing et al., 2011) has demonstrated that individual polymer chains are stretched and fractured on a relatively short time scale (order of milliseconds in the cited experiments), whereas changes in the mean molecular weight occur on a significantly longer time scale (order of tenths of seconds). This large time scale separation is ascribed to the fact that, at any instant in time, a relatively low percentage of polymer chains are significantly stretched. According to Vanapalli et al. (2006), polymer chain degradation under elongational flow is triggered by strain

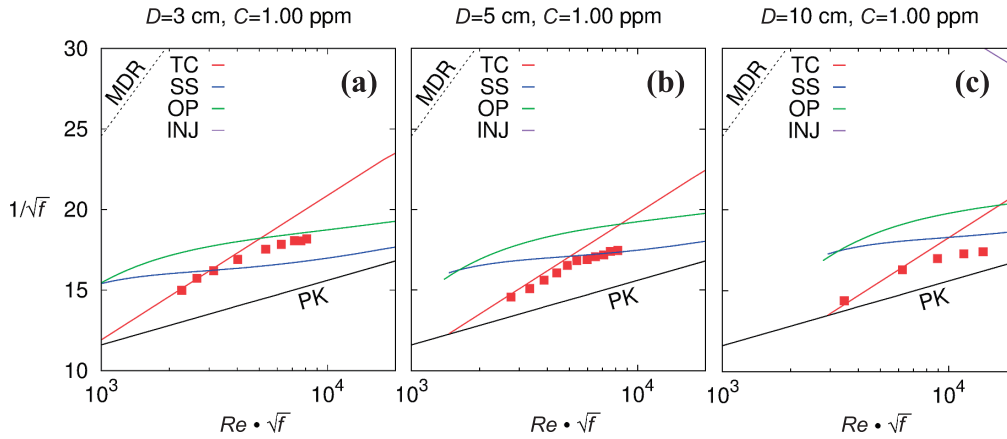


Fig. 10 Reference curves for DR prediction in industrial loop. TC (red line) is the theoretical line corresponding to the polymeric regime; OP (green line) is the curve corresponding to one-pass scission; SS (blue line) and INJ (purple line, visible only in the largest pipe) correspond to steady state scission and degradation due to the injection system, respectively. Symbols correspond to WSR-301 solution at the reference concentration of 1 ppm. Results from the Authors.

rates exceeding a threshold given by: $\dot{\epsilon}_D = D \cdot M_w^E$, where D and E are also coefficients, e.g. $E = 4.2651 \cdot 10^{10}$ and $D = -1.23$ for PEO; $D = 1.64737 \cdot 10^{11}$ and $E = -1.27$ for HPAM (Vanapalli et al., 2006). These data on polymer mechanical degradation can be used to identify and plot in P-K coordinates the limiting value of shear stress and elongational stress the polymer can be exposed to before being degraded by the flow. **Fig. 10** shows these curves together with the experimental data collected for PEO (WSR-301) at 1 ppm concentration in the three different pipes. TC (red line) is the theoretical line corresponding to the polymeric regime (Eq. 5); OP (green line) is the curve corresponding to one-pass scission; SS (blue line) corresponds to steady state scission and INJ (purple line, visible only in the largest pipe) corresponds to degradation produced by the injection system. The agreement between experimental data (red symbols) and reference curves for degradation is quite good and indicates that drag reduction in real systems can be predicted with some confidence also for situations in which $Re\sqrt{f} \geq (Re\sqrt{f})^*$. Mechanical degradation leads to the alteration of the molecular weight (Yang and Ding, 2013). To determine the local molecular weight of the injected polymer, Elbing et al. (2011) proposed the following scaling:

$$\frac{M_w - M_{ws}}{M_{wo}} = \exp[-8.6 \cdot 10^{-5} (t_f \cdot \gamma_w)] \quad (7)$$

where M_w is the local molecular weight, M_{ws} is the steady-state molecular weight (defined as the minimum M_w that can be obtained at a given γ_w), M_{wo} is the non-degraded value of M_w at the point of injection, and $t_f = (X - X_{inj})/U_\infty$ is the polymer residence time in the flow, $(X - X_{inj})$ being the distance travelled by the polymer, and U_∞ the convection velocity. **Fig. 11** shows the accuracy of this scaling for different characteristics of polymer degradation within a turbulent boundary layer. Changes in mean molecular

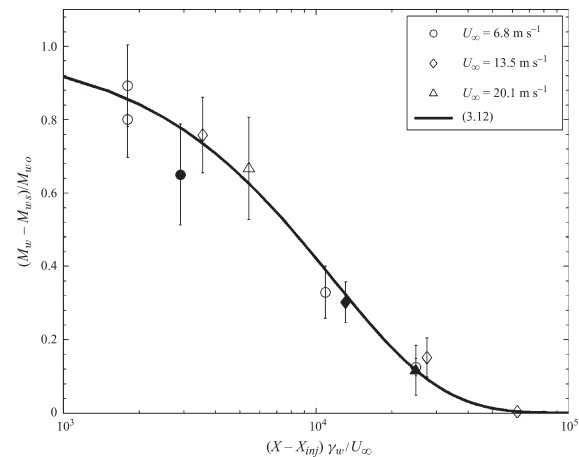


Fig. 11 Normalized difference between measured and steady-state molecular weights scaled with the product of residence time and wall shear rate. Results refer to rough (solid symbols) and smooth (open symbols) surfaces. The solid curve is the fit to the data and is provided by Eq. 7, namely Eq. (3.12) in Elbing et al. (2011). The error bars were determined from standard error propagation analysis. Reproduced with permission from Elbing et al. (2011).

weight occur on a time scale proportional to the polymer residence time. In addition, M_w tends to a finite level with increased residence time and shear rate, and the key parameters that control the degradation process appear to be the shear rate, polymer residence time in the TBL flow, M_{wo} and M_{ws} (Elbing et al., 2011).

6. Additive DR from a physico-chemical perspective

As mentioned in the previous section, mechanical degradation represents an important aspect of DR phenomena because of its practical implications for the design of accurate experiments (Wyatt et al., 2011). Mechanical deg-

radiation pertains the physico-chemical aspects of DR, which are in strong connection with the rheological and fluid mechanics aspects already covered. We believe that discussing physico-chemical aspects is thus important to provide a coherent picture of the intrinsic complexity of DR phenomena.

Regarding mechanical degradation, a crucial issue is the polymer resistance to chain scission, which poses an upper bound to the level of DR that can be achieved by the additive as well as the time/distance over which the additive is effective as drag reducer (see Choi et al., 2000; Elbing et al., 2009; Soares et al., 2015). When polymers are added to the flow as a homogeneous mixture in a wall-bounded flow, protocols (e.g. batch mixing by low shear impeller or tumble blenders, in line mixing by recirculation using low shear pumps, as in Campolo et al., 2015; Japper-Jaafar et al., 2009) are typically enforced during polymer mixture preparation to avoid mechanical degradation. When polymers are injected at the wall, small information is generally given on details of the injection system used which, per se, might induce degradation. Whichever the origin of mechanical degradation, the limiting value of the shear rate able to produce chain scission can be measured by experiments. Scaling relationships have been derived to link the limiting shear rate to the polymer molecular weight and to the strength of chemical bonds (Vanapalli et al., 2006). As demonstrated by Vanapalli et al. (2006), in a system properly designed to avoid any local degradation, the local stress at the Kolmogorov scale able to generate the molecular tension leading to polymer covalent bond breakage inside the pipe can be evaluated and the effect of polymer mechanical degradation can be accounted for. The loss of efficiency of the additive as the mechanical degradation proceeds has been analysed by Choi et al. (2000) in a rotating apparatus and by Soares et al. (2015) in pipe flow. Whichever the flow configuration, the physical mechanism governing degradation is independent of geometry. Kalashnikov (2002) found that for low enough additive concentration, the initial value of the friction coefficient and its variations in the course of degradation are also independent of the Weissenberg number. A half-degradation time can be defined from theoretical considerations and measured in connection with the flow hydrodynamics and network characteristics to estimate the span over which periodic polymer injection should be performed to maintain a desired level of DR.

A recent investigation focusing on the deformation of polymer molecules is reported in Shaban et al. (2018), who used planar PIV to gather detailed measurements of the turbulent flow field in a channel when polymers (PAM) are exploited as DRA. Their data, together with the rheological characterization (shear and elongational viscosity) of the polymeric solution allowed to character-

ize the interaction between the polymer molecules and turbulence. Measurements of mean flow, second-order turbulence statistics, and local strain-rate and rotation rate obtained using time-resolved 2D-PIV, showed that the extent of polymer deformation strongly depends on the wall-normal location, and is caused mainly by the streamwise strain rates. In the log-layer, polymer molecules do not exhibit significant stretching, since they were found to sample regions of strong rotation more often than regions of strong shear. At a high polymer concentration, rotation and shear were found to be in balance both in the buffer layer and in the log layer.

Another important physico-chemical aspect of DR is represented by the polymer microstructure, which nowadays can be designed ad-hoc to support the synthesis of well-defined macromolecules able to achieve desired supramolecular characteristics (D'hooge, 2015). Wever et al. (2013) used controlled synthesis to produce high molecular weight branched polyacrylamides, PAM, to be used as drag reducing agents. The equilibrium conformation of polymers having the same molecular weight but different microstructure were analysed using Dynamic Light Scattering (DLS) to measure their hydrodynamic volume; their intrinsic viscosity in solution was measured by viscosity tests. Results showed that the molecular architecture of more branched (13 and 17-arm PAMs) polymers was more extended in solution than that of their linear (4 and 8-arm analogues) counterpart; as a consequence, the elastic response of polymers solutions was enhanced, leading to an improved thickening efficiency that supported the use of branched PAMs for application in Enhanced Oil Recovery and DR. Controlling the microstructure of the polymer may also allow controlling its extensional viscosity, which according to many authors, can become much higher than the intrinsic viscosity (see Housiadas and Beris (2004) and references therein). An abrupt increase in the extensional viscosity that depends on the extensional strain rate is therefore deemed to be a key factor in turbulent DR (Hidema et al., 2013). Polymer-induced DR under different extensional strain rates have been analyzed by image processing calculating the curvature histogram of the interference pattern, which is related to the distribution of the velocity fluctuation. Results indicate that different processes of energy transfer reduction are activated depending on the polymer type (flexible/rigid). Flexible polymers are stretched and oriented parallel to the streamwise direction, whereas rigid rod-like polymers are only re-oriented parallel to the streamwise direction without extension. In the normal direction, the energy transfers are prohibited by orientated polymers. The stretching process of flexible polymers (PEO) increased the extensional viscosity, which also prohibits energy transfer in the streamwise direction (Shaban et al., 2018). Hidema et al. (2013) developed ad-hoc tests

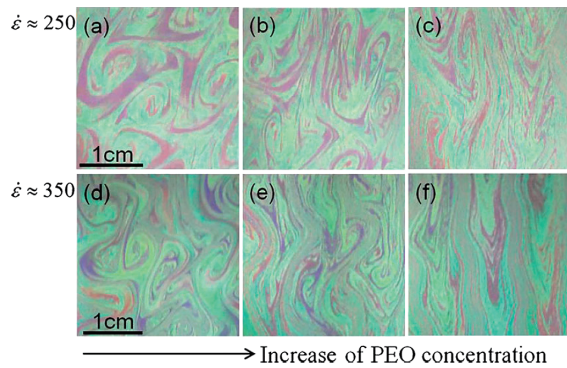


Fig. 12 Interference images of turbulence in flowing soap films of PEO solution at different extensional rates. Images refer to increasing PEO solution ($C = 0.5 \cdot 10^{-3}$ wt %, $1 \cdot 10^{-3}$ wt % and $2 \cdot 10^{-3}$ wt % from left to right) and increasing extensional rates ($\dot{\epsilon} = 250 \text{ s}^{-1}$ and 350 s^{-1} from top to bottom). Reproduced with permission from Hidema et al. (2013).

in two-dimensional turbulence made by flowing soap films to investigate DR by flexible polymers (e.g. PEO) and rod-like polymers (e.g. HPC, hydroxypropyl cellulose) in the absence of shear flow. Using a grid to generate extensional strain in a flowing solution containing polymers, Hidema et al. (2013) recorded the interference pattern of soap films with a video camera to observe the effect of polymer stretching and polymer re-orientation on 2D turbulence. **Fig. 12** shows the corresponding interference images of the turbulence in flowing soap films of PEO-added solution at different extensional rate.

7. Conclusions and future perspectives

The discussion proposed in this review highlights a number of crucial challenges for future research. Many experimental and numerical results indicate that the structure of a turbulent flow laden with polymers and/or fibers can be modified over a wide range of length scales even for very small concentrations of the additives. Additionally, effects due to additives depend strongly and not straightforwardly on the concentration: While the flow statistics in the dissipation range of turbulence change smoothly as a function of additive concentration, there is evidence that the inertial-range values of the structure functions are modified only when the concentration exceeds a specific threshold (which is flow and polymer-type dependent). Open issues are therefore related to the lack of a clearcut explanation of the qualitative change in the effect of the additive above the critical concentration, and to the need for a better understanding of the exact ways in which the additives affect the energy cascade. Considering that the time criterion for the onset of DR does not hold in the bulk of the flow, a physical mechanism by which the polymers can affect scales much larger than their size has yet to be identified. A promising route to

achieve this goal seems to be represented by the possibility to describe the effect of the polymer/fiber additive through models derived from viscoelastic turbulence theory. In terms of available scaling laws, it appears that more comprehensive datasets (both experimental and numerical) are needed to develop truly universal relations. Datasets need to be expanded by including a wider range of polymer types, molecular weights, injection conditions (for processes involving polymer degradation) and flow parameters to properly assess the universality of the scaling. This would lead to further improvement of existing correlations, which aim to predict mechanical degradation and the resulting loss of efficiency of drag reducers induced either by turbulence or by the injection system.

Acknowledgments

We are very grateful to Professor Soldati for the useful discussions.

References

- Adrian R.J., Meinhart C.D., Tomkins C.D., Vortex organization in the outer region of the turbulent boundary layer, *J. Fluid Mech.*, 422 (2000) 1–54. DOI: 10.1017/S0022112000001580
- Berman N.S., Drag reduction by polymers, *Annu. Rev. Fluid Mech.*, 10 (1978) 47–64. DOI:10.1146/annurev.fl.10.010178.000403
- Bhambri P., Narain R., Fleck B.A., Thermo-responsive polymers for drag reduction in turbulent Taylor-Couette flow, *J. Appl. Polymer Sci.*, 133 (2016) 44191. DOI: 10.1002/app.44191
- Blackburn H.M., Mansour N.N., Cantwell B.J., Topology of fine-scale motions in turbulent channel flow, *J. Fluid Mech.*, 310 (1996) 269–292. DOI: 10.1017/S0022112096001802
- Boelens A.M.P., Muthukumar M., Rotational relaxation time as unifying time scale for polymer and fiber drag reduction, *Phys. Rev. E*, 93 (2016) 052503. DOI: 10.1103/PhysRevE.93.052503
- Calzetta E., Drag reduction by polymer additives from turbulent spectra, *Phys. Rev. E*, 82 (2010) 066310. DOI: 10.1103/PhysRevE.82.066310
- Campolo M., Simeoni M., Lapasin R., Soldati, A., Turbulent drag reduction by biopolymers in large scale pipes, *ASME. J. Fluids Eng.*, 137 (2015) 041102. DOI: 10.1115/1.4028799
- Choi H.J., Kim, C.A., Sohn J.I., Jhon M.S., An exponential decay function for polymer degradation in turbulent drag reduction, *Polym. Degrad. Stab.*, 69 (2000) 341–346. DOI: 10.1016/S0141-3910(00)00080-X
- Choueiri G.H., Lopez J.M., Hof B., Exceeding the asymptotic limit of polymer drag reduction, *Phys. Rev. Lett.*, 120 (2018) 124501. DOI: 10.1103/PhysRevLett.120.124501
- de Chaumont Quiry A., Ouellette N.T., Concentration effects on turbulence in dilute polymer solutions far from walls, *Phys. Rev. E*, 93 (2016) 063116. DOI: 10.1103/PhysRevE.

- 93.063116
- de Gennes P.G., Introduction to Polymer Dynamics, Cambridge University Press, 1990. ISBN: 9780511569463. DOI: 10.1017/CBO9780511569463
- D'hooge D.R., Van Steenberghe P.H.M., Derboven P., Reyniers M.F., Marin G.B., Model-based design of the polymer microstructure: bridging the gap between polymer chemistry and engineering, *Polym. Chem.*, 6 (2015) 7081–7096. DOI: 10.1039/c5py01069a
- Dubief Y., Terrapon V.E., White C.M., Shaqfeh E.S.G., Moin P., Lele S.K., New answers on the interaction between polymers and vortices in turbulent flows, *Flow, Turbul. Combust.*, 74 (2005) 311–329. DOI: 10.1007/s10494-005-9002-6
- Dubief Y., White C.M., Terrapon V.E., Shaqfeh E.S.G., Moin P., Lele S.K., On the coherent drag-reducing and turbulence-enhancing behaviour of polymers in wall flows, *J. Fluid Mech.*, 514 (2004) 271D280. DOI: 10.1017/S0022112004000291
- Elbing B.R., Solomon M.J., Perlin M., Dowling D.R., Ceccio S.L., Flow-induced degradation of drag-reducing polymer solutions within a high-Reynolds number turbulent boundary layer, *J. Fluid Mech.*, 670 (2011) 337–364. DOI: 10.1017/S0022112010005331
- Elbing B.R., Winkel E.S., Solomon M.J., Ceccio S.L., Degradation of homogeneous polymer solutions in high shear turbulent pipe flow, *Exp. Fluids*, 47 (2009) 1033–1044. DOI: 10.1007/s00348-009-0693-7
- Elsnab J.R., Monty J.P., White C.M., Koochesfahani M.M., Klewicki J.C., High-fidelity measurements in channel flow with polymer wall injections, *J. Fluid Mech.*, 859 (2019) 851–886. DOI: 10.1017/jfm.2018.873
- Escudier M.P., Nickson A.K., Poole R.J., Turbulent flow of viscoelastic shear-thinning liquids through a rectangular duct: Quantification of turbulence anisotropy, *J. Non-Newtonian Fluid Mech.*, 160 (2009) 2–10. DOI: 10.1016/j.jnnfm.2009.01.002
- Flory P.J., Principles of Polymer Chemistry, 1 edition, Cornell University Press, 1953, ISBN: 0801401348.
- Fsadni A.M., Whitty J.P.M., Stables M.A., A brief review on frictional pressure drop reduction studies for laminar and turbulent flow in helically coiled tubes, *Appl. Therm. Eng.*, 109 (2016) 334–343. DOI: 10.1016/j.applthermaleng.2016.08.068
- Fu Z., Otsuki T., Motozawa M., Kurosawa T., Yu B., Kawaguchi Y., Experimental investigation of polymer diffusion in the drag-reduced turbulent channel flow of inhomogeneous solution, *Int. J. Heat Mass Tran.*, 77 (2014) 860–873. DOI: 10.1016/j.ijheatmasstransfer.2014.06.016
- Fujimura M., Iwamoto K., Murata A., Masuda M., Ando H., Mamori H., Influence of length of polymer aggregation on turbulent friction drag reduction effect, *J. Fluid Sci. Tech.*, 12 (2017). DOI: 10.1299/jfst.2017jfst0013
- Ganapathisubramani B., Longmire E.K., Marusic I., Characteristics of vortex packets in turbulent boundary layers, *J. Fluid Mech.*, 478 (2003) 35–46. DOI: 10.1017/S0022112002003270
- Ghosal A., Cherayil B.J., Anomalies in the coil-stretch transition of flexible polymers, *J. Chem. Phys.*, 148 (2018), 094903. DOI: 10.1063/1.5017555
- Gillissen J.J.J., Boersma B.J., Mortensen P.H., Andersson H.I., Fibre-induced drag reduction, *J. Fluid Mech.*, 602 (2008) 209–218. DOI: 10.1017/S0022112008000967
- Gillissen J.J.J., Hoving J.P., Self-similar drag reduction in plug-flow of suspensions of macroscopic fibers, *Phys. Fluids*, 24 (2012) 111702. DOI: 10.1063/1.4766198
- Graham M.D., Drag reduction and the dynamics of turbulence in simple and complex fluids, *Phys. Fluids*, 26 (2014) 101301. DOI: 10.1063/1.4895780
- Guan X.L., Yao S.Y., Jiang N., A study on coherent structures and drag-reduction in the wall turbulence with polymer additives by TRPIV, *Acta Mech. Sin.*, 29 (2013) 485–493. DOI: 10.1007/s10409-013-0035-0
- Han W.J., Dong Y.Z., Choi H.J., Applications of water-soluble polymers in turbulent drag reduction, *Processes*, 5 (2017) 24. DOI: 10.3390/pr5020024
- Hart A., A review of technologies for transporting heavy crude oil and bitumen via pipelines, *J. Petrol. Explor. Prod. Technol.*, 4 (2014) 327–336. DOI:10.1007/s13202-013-0086-0
- Hershey H.C., Zakin J.L., Existence of two types of drag reduction in pipe flow of dilute polymer solutions, *Ind. Eng. Chem. Fund.*, 6 (1967) 381–387. DOI: 10.1021/i160023a010
- Hidema R., Suzuki H., Hisamatsu S., Komoda Y., Furukawa H., Effects of the extensional rate on two-dimensional turbulence of semi-dilute polymer solution flows, *Rheol. Acta*, 52 (2013) 949–961. DOI: 10.1007/s00397-013-0733-3
- Housiadas K.D., Beris A.N., An efficient fully implicit spectral scheme for DNS of turbulent viscoelastic channel flow, *J. Non-Newtonian Fluid Mech.*, 122 (2004) 243–262. DOI: 10.1016/j.jnnfm.2004.07.001
- Japper-Jaafar A., Escudier M.P., Poole R.J., Turbulent pipe flow of a drag-reducing rigid “rod-like” polymer solution, *J. Non-Newtonian Fluid Mech.*, 161 (2009) 86–93. DOI: 10.1016/j.jnnfm.2009.04.008
- Jodai Y., Elsinga G.E., Experimental observation of hairpin auto-generation events in a turbulent boundary layer, *J. Fluid Mech.*, 795 (2016) 611–633. DOI: 10.1017/jfm.2016.153
- Jovanović J., Pashtrapanska M., Frohnapfel B., Durst F., Koskinen J., Koskinen K., On the mechanism responsible for turbulent drag reduction by dilute addition of high polymers: Theory, experiments, simulations, and predictions, *Trans. ASME*, 128 (2006) 118–130. DOI: 10.1115/1.2073227
- Kalashnikov V.N., Degradation accompanying turbulent drag reduction by polymer additives, *J. Non-Newtonian Fluid Mech.*, 103 (2002) 105–121. DOI: 10.1016/S0377-0257(01)00156-2
- Kim K., Adrian R.J., Balachandar S., Sureshkumar R., Dynamics of Hairpin Vortices and Polymer-Induced Turbulent Drag Reduction, *Phys. Rev. Lett.*, 100 (2008) 134504. DOI: 10.1103/PhysRevLett.100.134504
- Kim K., Li C.F., Sureshkumar R., Balachandar S., Adrian R.J., Effects of polymer stresses on eddy structures in drag-reduced turbulent channel flow, *J. Fluid Mech.*, 584 (2007) 281–299. DOI: 10.1017/S0022112007006611
- Lee J.H., Sung H.J., Very-large-scale motions in a turbulent

- boundary layer, *J. Fluid Mech.*, 673 (2011) 80–120. DOI: 10.1017/S002211201000621X
- Li C.F., Sureshkumar R., Khomami B., Simple framework for understanding the universality of the maximum drag reduction asymptote in turbulent flow of polymer solutions, *Phys. Rev. E*, 92 (2015) 043014. DOI: 10.1103/PhysRevE.92.043014
- Lumley J.L., Drag reduction by additives, *Annu. Rev. Fluid Mech.*, 1 (1969) 367–384. DOI: 10.1146/annurev.fl.01.010169.002055
- Lumley J.L., Drag reduction in turbulent flow by polymer additives, *J. Polym. Sci. Macromol. Rev.*, 7 (1973) 263–290. DOI: 10.1002/pol.1973.230070104
- Lumley J.L., Kubo I., Turbulent drag reduction by polymer additives: A survey. In: Gampert B. (eds) *The Influence of Polymer Additives on Velocity and Temperature Fields*. Springer, Berlin, Heidelberg, 1985, pp.3–21.
- Marchioli C., Soldati A., Mechanisms for particle transfer and segregation in a turbulent boundary layer, *J. Fluid Mech.*, 468 (2002) 283–315. DOI: 10.1017/S0022112002001738
- Moosaie A., Manhart M., An algebraic closure for the DNS of fiber-induced turbulent drag reduction in a channel flow, *J. Non-Newton. Fluid*, 166 (2011) 1190–1197. DOI: 10.1016/j.jnnfm.2011.07.006
- Moosaie A., Manhart M., Direct Monte Carlo simulation of turbulent drag reduction by rigid fibers in a channel flow, *Acta Mech.*, 224 (2013) 2385–2413. DOI: 10.1007/s00707-013-0919-x
- Ouellette N.T., Xu H., Bodenschatz E., Bulk turbulence in dilute polymer solutions, *J. Fluid Mech.*, 629 (2009) 375–385. DOI: 10.1017/S0022112009006697
- Owolabi B.E., Dennis D.J.C., Poole R.J., Turbulent drag reduction by polymer additives in parallel-shear flows, *J. Fluid Mech.*, 827 (2017) R4. DOI: 10.1017/jfm.2017.544
- Paschkewitz J.S., Dubief Y., Dimitropoulos C.D., Shaqfeh E.S.G., Moin P., Numerical simulation of turbulent drag reduction using rigid fibres, *J. Fluid Mech.*, 518 (2004) 281–317. DOI: 10.1017/S0022112004001144
- Paschkewitz J.S., Dubief Y., Shaqfeh E.S.G., The dynamic mechanism for turbulent drag reduction using rigid fibers based on Lagrangian conditional statistics, *Phys. Fluids*, 17 (2005) 1–18. DOI: 10.1063/1.1925447
- Picciotto M., Marchioli C., Soldati A., Characterization of near-wall accumulation regions for inertial particles in turbulent boundary layers, *Phys. Fluids*, 17 (2005) 098101. DOI: 10.1063/1.2033573
- Roy A., Larson R.G., A mean flow model for polymer and fiber turbulent drag reduction, *Appl. Rheol.*, 15 (2006) 370–389. <https://www.ar.ethz.ch/ARONLINE_FREE/15_370.pdf> accessed 13.04.2020.
- Samanta D., Dubief Y., Holzner M., Schafer C., Morozov A.N., Wagner C., Hof B., Elasto-inertial turbulence, *Proc. Natl. Acad. Sci. USA*, 110 (2013) 10557–10562. DOI: 10.1073/pnas.1311539110
- Shaban S., Azad M., Trivedi J., Ghaemi S., Investigation of near-wall turbulence in relation to polymer rheology, *Phys. Fluids*, 30 (2018) 125111. DOI: 10.1063/1.5062156
- Shahmardi A., Zade S., Ardekani M.N., Poole R.J., Lundell F., Rosti M.E., Brandt L., Turbulent duct flow with polymers, *J. Fluid Mech.*, 859 (2019) 586–612. DOI: 10.1017/jfm.2018.858
- Sher I., Hetsroni G., A mechanistic model of turbulent drag reduction by additives, *Chem. Eng. Sci.*, 63 (2008) 1771–1778. DOI: 10.1016/j.ces.2007.11.035
- Shetty A.M., Solomon M.J., Aggregation in dilute solutions of high molar mass poly(ethylene) oxide and its effect on polymer turbulent drag reduction, *Polymer*, 50 (2009) 261–270. DOI: 10.1016/j.polymer.2008.10.026
- Soares E.J., Sandoval G.A.B., Silveira L., Pereira A.S., Trevelin R., Thomaz F., Loss of efficiency of polymeric drag reducers induced by high Reynolds number flows in tubes with imposed pressure, *Phys. Fluids*, 27 (2015) 125105. DOI: 10.1063/1.4937594
- Somani S., Shaqfeh E.S.G., Prakash J.R., Effect of solvent quality on the coil-stretch transition, *Macromolecules*, 43 (2010) 10679–10691. DOI: 10.1021/ma1019945
- Sreenivasan, K.R., White C., The onset of drag reduction by dilute polymer additives, and the maximum drag reduction asymptote, *J. Fluid Mech.*, 409 (2000) 586–612. DOI: 10.1017/s0022112099007818
- Tabor M., De Gennes P.G., A cascade theory of drag reduction, *Europhys. Lett.*, 2 (1986) 519–522. DOI: 10.1209/0295-5075/2/7/005
- Teng H., Liu N.S., Lu X.Y., Khomami B., Turbulent drag reduction in plane Couette flow with polymer additives: a direct numerical simulation study, *J. Fluid Mech.*, 846 (2018) 482–507. DOI: 10.1017/jfm.2018.242
- Tiong A.N.T., Kumar P., Saptoro A., Reviews on drag reducing polymers, *Korean J. Chem. Eng.*, 32 (2015) 1455–1476. DOI: 10.1007/s11814-015-0104-0
- Valente P.C., da Silva C.B., Pinho F.T., The effect of viscoelasticity on the turbulent kinetic energy cascade, *J. Fluid Mech.*, 760 (2014) 39–62. DOI: 10.1017/jfm.2014.585
- Vanapalli S.A., Ceccio S.L., Solomon M.J., Universal scaling for polymer chain scission in turbulence, *Proc. Natl. Acad. Sci. USA*, 103 (2006) 16660–16665. DOI: 10.1073/pnas.0607933103
- Virk P.S., Drag reduction fundamentals, *AIChE J.*, 21 (1975) 625–656. DOI: 10.1002/aic.690210402
- Voth G.A., Soldati A., Anisotropic particles in turbulence, *Annu. Rev. Fluid Mech.*, 49 (2017) 249–276. DOI: 10.1146/annurev-fluid-010816-060135
- Wang S.N., Graham M.D., Hahn F.J., Xi L., Time-series and extended Karhunen-Loeve analysis of turbulent drag reduction in polymer solutions, *AIChE J.*, 60 (2014) 1460–1475. DOI: 10.1002/aic.14328
- Wever D.A.Z., Picchioni F., Broekhuis A.A., Branched polyacrylamides: Synthesis and effect of molecular architecture on solution rheology, *Eur. Polym. J.*, 49 (2013) 3289–3301. DOI: 10.1016/j.eurpolymj.2013.06.036
- White C.M., Dubief Y., Klewicki, J. Properties of the mean momentum balance in polymer drag-reduced channel flow, *J. Fluid Mech.*, 834 (2018) 409–433. DOI: 10.1017/jfm.2017.72
- White C.M., Mungal M.G., Mechanics and prediction of turbulent drag reduction with polymer additives, *Annu. Rev.*

- Fluid Mech., 40 (2008) 235–256. DOI: 10.1146/annurev.fluid.40.111406.102156
- Winkel E.S., Oweis G.F., Vanapalli S., Dowling D.R., Perlin M., Solomon M.J., Ceccio S.L., A high-Reynolds-number turbulent boundary layer friction drag reduction from wall-injected polymer solutions, *J. Fluid Mech.*, 621 (2009) 259–288. DOI: 10.1017/S0022112008004874
- Wyatt N.B., Gunther C.M., Liberatore M.W., Drag reduction effectiveness of dilute and entangled xanthan in turbulent pipe flow, *J. Non-Newtonian Fluid Mech.*, 166 (2011) 25–31. DOI: 10.1016/j.jnnfm.2010.10.002
- Xi H.D., Bodenschatz E., Xu H., Elastic energy flux by flexible polymers in fluid turbulence, *Phys. Rev. Lett.*, 111 (2013) 024501. DOI: 10.1103/PhysRevLett.111.024501
- Xi L., Bai X., Marginal turbulent state of viscoelastic fluids: A polymer drag reduction perspective, *Phys. Rev. E*, 93 (2016) 043118. DOI: 10.1103/PhysRevE.93.043118
- Xi L., Graham M.D., Turbulent drag reduction and multistage transitions in viscoelastic minimal flow units, *J. Fluid Mech.*, 693 (2012) 421–452. DOI: 10.1017/S0022112010000066
- Yang S.Q., Ding D.H., Drag reduction induced by polymer in turbulent pipe flows, *Chem. Eng. Sci.*, 102 (2013) 200–208. DOI: 10.1016/j.ces.2013.07.048
- Yang S.-Q., Dou G. Turbulent drag reduction with polymer additive in rough pipes, *J. Fluid Mech.*, 642 (2010) 279–294. DOI: 10.1017/S002211200999187X
- Zhang X., Duan X.L., Muzychka Y., Analytical upper limit of drag reduction with polymer additives in turbulent pipe flow, *J. Fluids Eng.*, 140 (2018) 051204. DOI: 10.1115/1.4038757
- Zhou Y., Schroeder C.M., Single polymer dynamics under large amplitude oscillatory extension, *Phys. Rev. Fluids*, 1 (2016) 053301. DOI: 10.1103/PhysRevFluids.1.053301

Authors' Short Biographies



Cristian Marchioli

Cristian Marchioli is Associate Professor of Fluid Mechanics at the University of Udine, Editor of *Acta Mechanica* and former chairman of the COST Action “Fiber suspension flow modeling”. Currently, Prof. Marchioli sits in the scientific council of the International Center of Mechanical Sciences, where he coordinated several advanced schools on particles in turbulence. His research interests involve multiphase flow modeling, from small-scale particle-turbulence interactions to large-scale modeling of gas-solid/gas-liquid flows. Prof. Marchioli has published 50+ papers and 100+ conference proceedings. He has also delivered several invited and keynote lectures at international conferences.



Marina Campolo

Marina Campolo is Associate Professor in Chemical Engineering at the University of Udine. She received her Laurea (M.S. - B.S.) in Industrial Engineering and got her Ph.D. in 1999 in Chemical Engineering from the University of Udine. Her research interests are in the area of process and environmental engineering with an emphasis on multiphase systems. Prof. Campolo has published 30+ papers and 50+ conference proceedings. Together with A. Soldati and A. Cremese, she received the 2007 Knapp award from the American Society of Mechanical Engineers.